

Operando Investigation of Al Plating Regimes on HOPG in [EMImCl]:AlCl₃ by Electrochemical Reflection Anisotropy Spectroscopy

Mario Löw^{*[a]} and Matthias M. May^[a, b]

Rechargeable aluminium batteries show promise as next-generation systems with a more abundant material base than lithium technology. However, the stable native oxide on top of aluminium metal electrodes leads to poor cell performance. Graphite, on the other hand, is a so far rarely investigated alternative that can be used as both the anode and cathode. Here, metallic aluminium is deposited at the anode, while AlCl₄⁻ is intercalated at the cathode. For both cases, understanding the electrode–electrolyte interface is crucial for improving the performance of the battery. In this work, we use reflection anisotropy spectroscopy to study the evolution of the interface

under applied potentials. We find that the cathode exhibits an irreversible swelling of the topmost graphite layer due to AlCl₄⁻ intercalation as well as the formation of an SEI during the first voltammetry cycle. On the anode, the electrodeposition of aluminium is initially well-ordered. However, the evolution of the surface morphology depends on the applied potential, with island-like growth at less cathodic potentials, and layer-by-layer growth at more anodic potentials. With the optical *operando* spectroscopy, we can follow these qualitatively different plating and stripping regimes in a time-resolved manner.

Introduction

Rechargeable aluminium batteries (RABs) are a promising material system for the battery market.^[1] Their advantages are the inexpensive, abundant, and recyclable aluminium as well as its high theoretical volumetric capacity of 8046 Ah L⁻¹,^[2] which is four times higher compared to the volumetric capacity of lithium (2062 Ah L⁻¹).^[3] Furthermore, its electronegativity is higher compared to other metals used as anode material. This suggests less reactivity and higher safety, meaning it can in principle be handled even when exposed to humid air.^[3] However, aluminium metal electrodes face the drawback of being covered with a native oxide layer consisting of the ion- and electron-blocking Al₂O₃.^[4] While the oxide layer can enhance the stability of the electrode/electrolyte interface and prevent dendrite formation,^[5] it might also impede the plating and stripping of aluminium in non-corrosive and non-acidic electrolytes without AlCl₃.^[6]

This combination of potential benefits with many remaining challenges for the RAB technology has resulted in significantly

increased interest in these systems over the last few years. This includes the development of organic red-ox molecules as cathode material^[7] or AlCl₃-free electrolytes.^[8] Further works targeted aluminium-sulphur,^[9] aluminium-selenium^[10] and aluminium-air batteries,^[11] including aqueous systems.^[12]

A promising, but rarely investigated alternative anode material is graphite. Its advantages are its low cost, high electrical conductivity, low density, and high-temperature resistance. A previous investigation showed that stripping and plating of aluminium from AlCl₃:BMImCl 2:1 onto expanded graphite is possible with high reversibility. The authors showed that the aluminium can be plated with an overpotential of only -80 mV. In addition, the plating-stripping charge efficiency was 84%, close to the value they obtained for an aluminium metal anode.^[13] A further advantage of graphite for RABs is that it can simultaneously be used as an anode and cathode. This is the case since it works with two distinct mechanisms, depending on the polarisation of the electrode. On the cathode side, ions are intercalated/deintercalated into the host lattice. On the anode side, aluminium is stripped and plated onto the graphite. Such a mode of operation also does not require the anode or the cathode to contain Al in the first place. It only needs a material that is an efficient current collector on the anode side and good intercalation material on the cathode side.

Such a kind of battery has already been experimentally demonstrated.^[14,15] In these studies, conductive graphite paper was used as the anode and cathode and EMImCl:AlCl₃ as the electrolyte. Due to the high ionic conductivity of the electrolyte, this battery shows a reasonable rate and cycle performance of up to 1000 cycles. The initial discharge capacity is around 70 mAh g⁻¹ at a current density of 200 mA g⁻¹. The battery also provides a discharge voltage of 2.1 V (vs. Al³⁺/Al). However, the drawback of this kind of battery is strong self-discharge, with

[a] M. Löw, M. M. May
Institute of Theoretical Chemistry, Universität Ulm, Lise-Meitner-Str. 16,
89081 Ulm, Germany
E-mail: mario.loew@uni-ulm.de

[b] M. M. May
Institute of Physical and Theoretical Chemistry, Universität Tübingen,
Auf der Morgenstelle 15, 72076 Tübingen, Germany

 Supporting information for this article is available on the WWW under
<https://doi.org/10.1002/batt.202400610>

 © 2024 The Author(s). Batteries & Supercaps published by Wiley-VCH GmbH.
This is an open access article under the terms of the Creative Commons Attribution License, which permits use, distribution and reproduction in any medium, provided the original work is properly cited.

16.82%/h in the mentioned publication. Such a system is called a rechargeable dual-carbon battery (RDCB) and the principle is also known for lithium and sodium.^[16,17]

Both the cathode as well as the anode have already been investigated before. However, on the cathode side, the focus was the intercalation of the AlCl_4^- into the graphite host.^[18] Computational studies show that the intercalation of AlCl_4^- into graphite is a four-step process and that, due to the tetrahedral form of the AlCl_4^- , the graphite layers get distorted.^[19] The cathode–electrolyte interface has, despite carbon also being used in Al–carbon batteries,^[20] only been investigated by Canever et al.^[21] The authors discovered that an interfacial layer is formed on the cathode in the first cycle, where the electrolyte decomposes at potentials lower than 2.45 V. The cause for this layer are defects in the graphite and heteroatomic functional groups on the surface of the graphite.

For the anode, the stripping and plating of aluminium from ionic liquids such as [EMImCl]: AlCl_3 have been investigated in numerous studies, however mostly with metallic aluminium as substrate.^[22–26] The electrodeposition at the anode involves the Al_2Cl_7^- species, which can only be found in the electrolyte if the molar ratio of [EMImCl] and AlCl_3 is between 1:1 and 1:2.^[27] The electrodeposition mechanism of Al is governed by kinetics with diffusion control at the early stages. Thereby, the activation barrier and the standard equilibrium potential of the (de)chlorination reaction are the most important criteria for the electrodeposition of aluminium.^[22] In addition, the Al deposition is a multiple-step process, with either a chemical step ($\text{AlCl}_3^- \rightarrow \text{AlCl}_2 + \text{Cl}^-$) or an electron transfer ($\text{Al}^{2+} + \text{e}^- \rightarrow \text{Al}^+$) being the rate-determining step.^[24] Further, the addition of 1,10-phenanthroline anhydrate (OP) to the [EMImCl]: AlCl_3 leads to smoother Al deposition.^[25]

The highly-oriented pyrolytic graphite (HOPG), that we used in our investigation, has already been studied for the electrodeposition of several metals. This is because electrochemical metal deposition represents a suitable and straightforward approach for local surface structuring and modification and allows the preparation of a surface for the investigation of potential catalysts.^[28] Work on Pt showed that the morphology of the deposited Pt nano-particles depends strongly on the applied potential and the current density.^[29,30] Further studies were also conducted with Ag,^[31] Hg^[32] and Pd.^[33]

For battery anode materials, there is a large number of *operando*, time-resolved investigations on electrodeposition, investigating potential dendrite formation with a focus on Li.^[34] Understanding the evolution of the surface morphology with applied anodic potentials is a crucial step for detecting potential dendrite growth. A smooth surface is less likely to cause short circuits inside the battery. Recent studies on the morphology of Mg electrodeposition show that its morphology is highly dependent on the used electrolyte. The Grignard electrolyte MeMgCl shows unidirectional growth and mossy deposition. $\text{Mg}[\text{B}(\text{HFIP})_4]_2$, on the other hand, did not show the formation of dendrites, yet the deposition was not smooth, either.^[35] An investigation by She et al.^[36] on the electrodeposition of aluminium with *in situ* optical microscopy and transmission electron microscopy showed that the shape of

dendritic Al deposits changes as a function of the current density. The deposits have a sharp tip shape at low current densities, while they have a spherical shape at high current densities. This change in morphology is due to the influence of the (local) current density on the movement of ions. When the current density is low, ions move slowly, creating a significant concentration gradient near the tip of dendritic Al. However, ions move more quickly at higher current densities, forming dendritic Al due to increased charge aggregation. A study by Ding et al.^[37] showed that high shear modulus metals can form globular dendrites – spherically deposited metal – which can penetrate the separator and cause a short circuit.

Despite numerous research on the electrodeposition of metals on HOPG, results on Al are rare. Tu et al. investigated the electrodeposition of Al on graphite from AlCl_3^- 1-butyl-3-methyl-imidazolium chloride (AlCl_3^- [Bmim]Cl).^[38] They discovered that the morphology of the deposited Al is dependent on the applied current density with coarse deposits at low current density and a more smooth surface at high current density. In addition, the increase in the current density leads to a decrease in the grain size of the deposited Al. The authors also investigated the crystallographic orientation and discovered that the X-ray diffraction peak intensity of the (200)-plane increases with increasing current density, while it decreases for the (111)-plane. This means that the current density has a significant influence on the crystallographic orientation of the deposited aluminium.^[38] Analysis of the electrodeposition was, however, mostly based on *ex situ* methods or with the mathematical model by Scharifker and Hills.^[39]

Operando spectroscopy, on the other hand, is typically preferable for electrochemical systems as it can ideally deliver time-resolved information on the involved processes as a function of the applied potential.^[40] For this investigation, we use reflection anisotropy spectroscopy (RAS) as an optical, time-resolved probe of the interfacial structure. RAS is a non-destructive optical light probe that investigates changes on the surface related to surface chemistry, such as adsorption/deposition or surface reconstruction, with a near-normal incidence reflection set-up.^[41] In previous studies, RAS has already been used for controlling the growth during metal-organic vapour deposition (MOCVD),^[42] surface etching and plating and stripping on aluminium^[43] and for controlling the layer-by-layer etching of multilayered semiconductors.^[44] Though so far rarely used in the battery field, RAS has the potential to provide insight into SEI formation, metal stripping/plating, as well as ion transport processes combining very high interface sensitivity with suitable time resolution. In order to measure RAS, linearly polarized light impinges at near-normal incidence on a single-crystalline surface. Then, the difference in reflectivity (Δr) with respect to the orthogonal directions in the surface plane (x, y) is normalized to the mean reflectivity, r .^[41] The surface's optical anisotropy is then defined as follows:

$$\text{RAS} := \Re\left(\frac{\Delta r}{r}\right) = 2 \cdot \frac{r_x - r_y}{r_x + r_y}; r \in \mathbb{C} \quad (1)$$

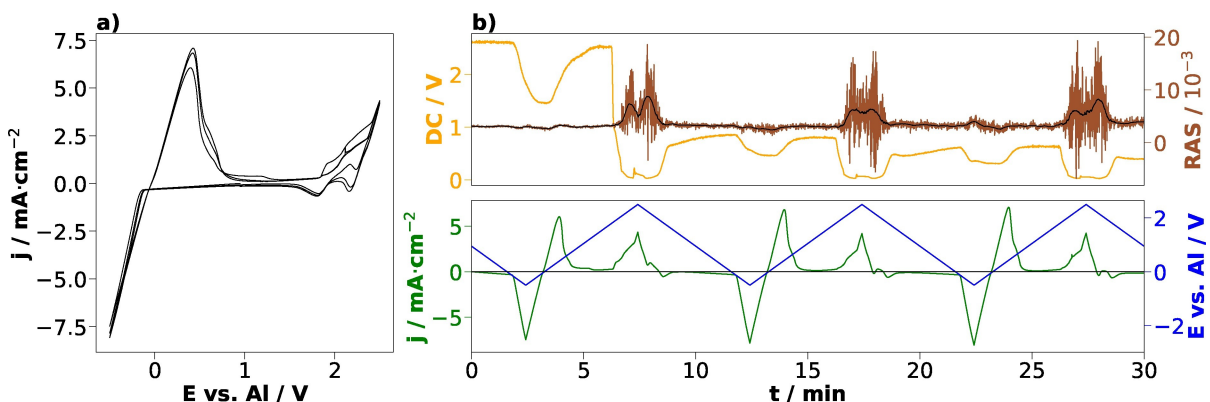


Figure 1. Optical signal during cycling in the full potential window and cyclic voltammogram. a) CV between -0.5 and 2.5 V (vs. Al pseudo-reference), starting from open circuit voltage (OCV) (0.9 V) towards the negative terminus at a scan speed of 10 mVs^{-1} for 3 cycles. b) Upper part: DC signal and transient at 1.5 eV photon energy. The black curve corresponds to the Savitzky–Golay-filtered transient. Lower part: Voltage and current density of the CV in a) plotted against time.

Due to light's penetration depth, both the surface and the bulk contribute to the signal. However, the highly-oriented pyrolytic graphite crystal employed here has the surface orientation (0001), meaning that it is optically isotropic; therefore, only changes on top of the surface contribute to the signal.

In this study, we investigate two different aspects of a dual-graphite battery, namely the interface of the cathode during the interaction of AlCl_4^- into graphite and the electrodeposition of aluminium onto HOPG. To this end, we used one of the most common electrolytes for rechargeable Al batteries, [EMImCl]: AlCl_3 (1:1.5). Both intercalation and electrodeposition were first investigated time-dependently with RAS during cyclic voltammetry (CV). Later, the electrodeposition of Al was investigated in depth by chronoamperometry (CA) and chronocoulometry (CC) measurements. The hereby electrodeposited Al is additionally investigated with scanning electron microscopy (SEM) and energy-dispersive X-ray spectroscopy (EDX) for a detailed understanding of the surface morphology. This allows us to observe an irreversible swelling of the topmost graphite layer as well as the formation of an SEI during the intercalation of AlCl_4^- into the graphite structure. Furthermore, we find that the deposition mechanism of Al on HOPG depends on the applied potential and has an ordered nucleation step at the beginning, while the microscopic stripping process depends on the prior plating mechanism.

Results and Discussion

The following section is separated into two parts. In the first one, we investigate the surface during the intercalation of AlCl_4^- into the layers of the HOPG. In the second part, we investigate the stripping and plating of metallic aluminium on top of the HOPG surface.

Intercalation and Deintercalation

Figure 1a shows the CV of HOPG in contact with EMImCl: AlCl_3 . The CV can be divided into two parts, which represent two different processes. The first part is the stripping and plating of aluminium; this can be found below 1.5 V (vs. Al pseudo-reference). The plating of aluminium is the cathodic process observed below 0 V, while stripping of aluminium is the anodic process above 0 V. The second process is the intercalation and de-intercalation of AlCl_4^- into the layers of the HOPG, occurring above 1.5 V.

Figure 1b shows a transient, which is the time-resolved optical signal at fixed photon energy, in this case recorded at 1.5 eV in parallel to the CV in Figure 1a. The DC signal, proportional to the reflectance, is shown in orange. It shows a decrease in reflectance while plating of aluminium and intercalation of AlCl_4^- . The most prominent decrease in reflectivity occurs the first time the potential surpasses 1.8 V. Here, we observe a substantial reduction in reflectance, which subsequently stays significantly below its initial value. This might be caused by the swelling of the topmost layer of graphite due to intercalation of AlCl_4^- . An expansion of the natural graphite due to AlCl_4^- intercalation has already been investigated before.^[20] Since the reflectance does not return to its original value, it is a clear indicator that this swelling or solid-electrolyte interphase (SEI) formation is irreversible. The following two cycles, in which the voltage surpasses 1.8 V, also show a reduction in reflectance. This time, it is less significant and returns almost to the initial value. This indicates that subsequent intercalation after the first irreversible swelling/SEI formation also changes the surface of the HOPG, either by reversible swelling or adsorption of the solvation shell of the intercalated ions.

The brown curve in Figure 1b shows the RA signal, a measure for the optical anisotropy of the surface, which shows a change in the anisotropy during the intercalation process around the maximum of the associated anodic current. The changes in the RA signal could in principle also arise from the

relatively low DC signal. However, applying the Savitzky-Golay-Filter to the data shows that two distinct positive peaks arise in all three intercalation steps, with the local minimum located at the turning point of the CV. This suggests that during intercalation of AlCl_4^- , an anisotropy is imposed on the interface between HOPG and electrolyte or in the arrangement of the AlCl_4^- underneath the first graphene layer. Theoretical calculations indicate that the bridge 2 position, where Al-anions occupy the bridging position between two non-bonded carbon atoms and the four Cl-atoms nearly occupy the center of the hexagon (C6), is the thermodynamically most stable position.^[19] This suggests that most of the intercalated AlCl_4^- went to this position. However, the other possible positions are also favourable, due to their energetic difference of below 0.02 eV.^[19] This could explain the dip in the optical anisotropy at the maximum anodic potential, where sites associated with anisotropy are occupied first and cleared last. Another possible explanation could be an ordered adsorption of AlCl_4^- or its solvation shell on top of the graphite.^[21]

Since the anodic current peak above 1.8 V could in principle be either caused by intercalation or graphite oxidation,^[20] we performed the same experiment with a glassy carbon electrode, to test our hypothesis. The CV of the glassy carbon still shows the stripping and plating peaks; however, above 1.8 V, no anodic waves are to be found (see SI Figure S1). This suggests that indeed, intercalation takes place above 1.8 V (vs. Al pseudo-reference).

For a more detailed investigation of the surface during intercalation, the HOPG sample was investigated with SEM/EDX after the three intercalation cycles stopped at open-circuit voltage (OCV). The SEM image shows a mosaic-like structure on the surface. Further analysis with EDX shows that this mosaic structure contains carbon, chloride, aluminium, and oxygen species. These either originate from a potential decomposition of the electrolyte or from molecular adsorption on the surface. A similar surface film was also observed by Canever et al.^[21] The authors claim that this surface film stems from the decomposition of the electrolyte, which can happen already below 2.5 V, depending on the type of carbon used. However, they also claim that this surface film is more likely to form on carbon surfaces with a high number of defects.^[21] HOPG, however, has a quite low number of defects. Similar phenomena are also already known from dual-ion lithium batteries.^[45] A mosaically structured SEI on carbon is also detected on the graphite anodes in lithium ion batteries.^[46]

For comparison, we cycled only until 1.5 V (vs. Al pseudo-reference) and investigated the resulting surface by means of SEM/EDX. The results are shown in Figure S4 in the SI. To avoid destruction of a potential SEI layer on top of the sample, we did not rinse it with THF (Tetrahydrofuran), as we did for all other samples. This, however, leads to residuals of the electrolyte being present on the surface. Yet still, no SEI can be observed on the surface.

From these results, we can summarize that both, intercalation of AlCl_4^- into graphite, and the irreversible formation of a surface layer are also associated with a distinct optical signature. The strong decrease in reflectance could, therefore,

be caused by the irreversible swelling of the graphite layer due to AlCl_4^- intercalation and the irreversible formation of a surface film on top due to a chemical reaction between the carbon and the electrolyte. The ex situ SEM/EDX investigation shows that this layer is stable outside the electrolyte and cannot be removed by washing the electrode in THF. The reduction in reflectance in the following two cycles might be caused by reversible adsorption on top of an already-formed surface layer or reversible intercalation since here, the reflectance returns to its original value. The anisotropy can be caused both by the ordered adsorption of AlCl_4^- (or the remainder of its solvation shell) on top of the surface or by its ordered intercalation. The swelling of the graphite structure and the SEI formation can actually be beneficial for the battery since the literature shows that the swelling of the graphite causes partially turbostratic structures and gradually forms new defects inside the graphite, resulting in the gradual increase of the capacity.^[47] The formation of an SEI on the graphite does, on the other hand, lead to a decrease in specific capacity after the first cycle and a simultaneous increase of the coulombic efficiency between the first and the second cycle.^[21]

It should be noted that due to our cell set-up, only the topmost layer is in contact with the electrolyte, meaning AlCl_4^- intercalation is only possible through defects in this layer. However, the same experiment with glassy carbon does not show any features in the CV, meaning that no intercalation or (electro)chemical reaction takes place. This could also mean that the formation of the irreversible surface layer requires the intercalation of AlCl_4^- into the graphite.

Stripping and Plating

We now turn to the stripping and plating of aluminium onto HOPG. To this end, we electrochemically cycled the HOPG between -0.5 V and 1.5 V, starting from OCV (1.6 V) towards the negative terminus, with a scan rate of 10 mVs^{-1} for ten cycles, while a transient with a photon energy of 1.5 eV was recorded. The results are shown in Figure 2.

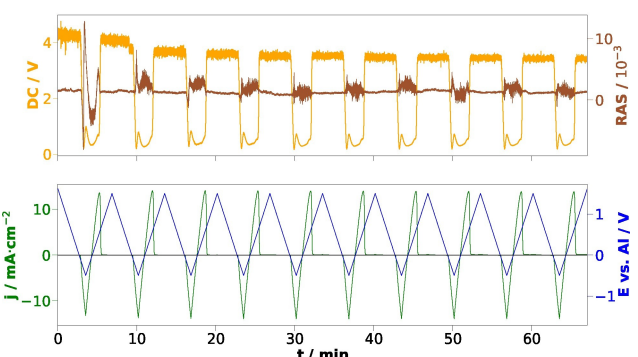


Figure 2. Optical signal during cycling in stripping and plating potential window and cyclic voltammogram. Upper part: DC signal and transients at 1.5 eV photon energy. Lower part: CV between -0.5 and 1.5 V (vs. Al pseudo-reference), starting from OCV (1.6 V) towards the negative terminus, with a scan rate of 10 mVs^{-1} for ten cycles.

The reflectance (orange curve) shows a similar behaviour as the previous measurement. It decreases upon plating aluminium and increases upon stripping. An interesting observation is a small peak during the plating process, in which the reflectance shortly increases and then decreases again. This peak always occurs at the negative terminus of -0.5 V (vs. Al pseudo-reference), in all of the ten CV cycles. This could indicate a change in how the aluminium is plated. The anisotropy (brown curve) strongly changes in the first cycle. Here, the anisotropy first decreases when the potential is below 0.2 V. During this change, a change in signs from positive to negative occurs. Further, the anisotropy increases again back to positive values; this happens simultaneously with the slight dip observed in the reflectance spectrum. During stripping, the anisotropy has a slight dip in positive direction before it returns to its initial value. This indicates an ordered deposition of the aluminium, taking place over three stages before the aluminium is stripped off again. Changes in the anisotropy also happen in the subsequent cycles; however, there, the changes are much smaller and less pronounced. A potential reason for this might be a decay of the topmost surface layer in contact with the electrolyte, also indicated by the slight decay of the plateau in the reflectance signal with continuous cycling.

For a more detailed view on this presumably ordered nucleation, a chronoamperometry (CA) measurement was performed. For that, the potential was set from OCV towards -0.5 V (vs. Al pseudo-reference) and held for 15 s. Afterwards, the potential was switched back to OCV again. During the whole time, a transient at a photon energy of 1.5 eV was recorded. The results can be seen in Figure 3a.

We observe that upon switching the potential from OCV to 0.5 V, the reflectance and the anisotropy follow instantaneously. In addition, there is a small peak at around 40 s for both, the anisotropy and the reflectance. This might originate from a change in the deposition mechanism of Al, but further investigations are needed to confirm this.

After going back to OCV, the anisotropy and the reflectance stay constant. Figure S5 (Supporting Information) shows RA-spectra of the clean HOPG sample as well as after the Al deposition, both outside of the electrolyte. The spectrum after the deposition is shifted downwards compared to the one with HOPG. In the area between 1.5 eV and 3.0 eV, the downward shift is more pronounced than for the rest of the spectra. This experiment also shows that the deposited Al is stable outside the electrolyte and its surface morphology can be investigated further with ex situ SEM.

Figure 3b and 3c displays an SEM image of the HOPG surface after Al deposition. It shows well-defined, isolated Al-particles spread across the whole surface. The higher magnification in b shows that the particles have a size of around $200\text{--}300$ nm. Additionally, some of the particles have a triangular shape with flattened corners. The triangular – or, more precisely, truncated octahedral – shape from the top-view of the face-centered cubic (fcc) crystal lattice suggests crystalline nucleation with a predominantly (111) surface,^[48,49] an ordering which is detectable by RAS. However, for a precise statement, it should be noted that the triangular-shaped particles also need

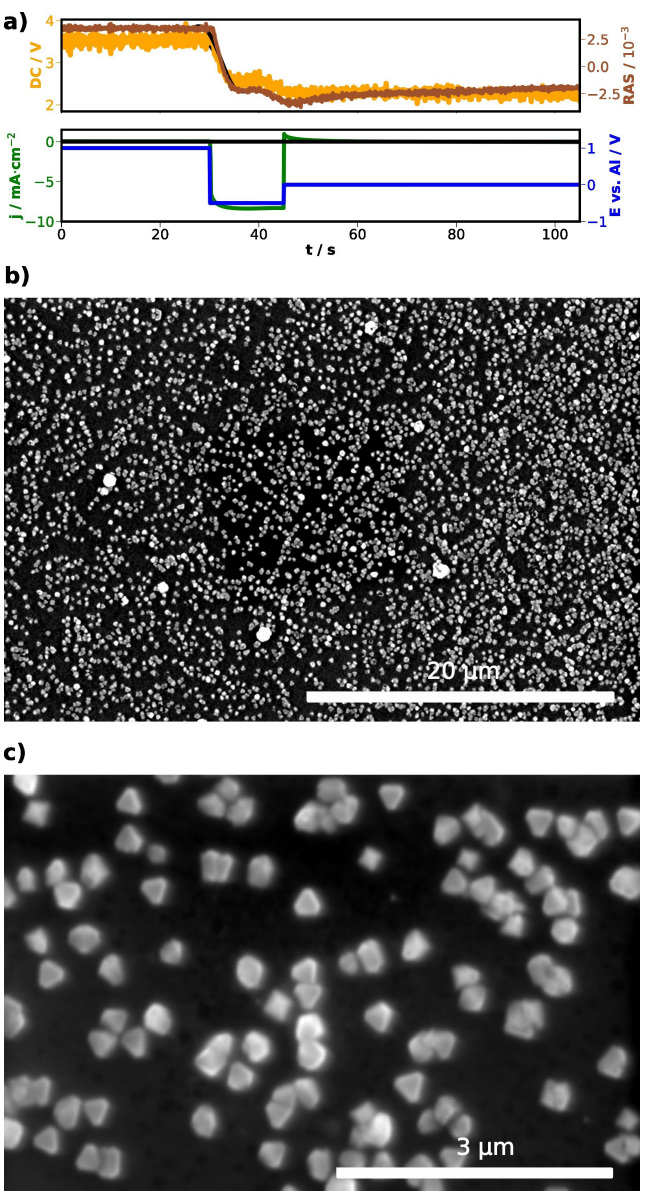


Figure 3. Optical signal during electrodeposition of Al at -0.5 V and ex situ SEM afterwards. a) Upper part: DC and RA transients at 1.5 eV photon energy. Lower part: CA OCV (30 s) \rightarrow -0.5 V (vs. Al pseudo-reference) (15 s) \rightarrow OCV. The black curve corresponds to the Savitzky-Golay-filtered transient. SEM of the HOPG sample after Al deposition at b) $5,000\times$ magnification and c) $30,000\times$ magnification.

to have a preferential orientation to contribute to the RAS signal. While initial inspection suggests that there is indeed a preferential orientation of the particles on the graphite substrate, a more quantitative analysis will have to be left to future work. Randomly oriented particles would average out over the optical measurement area of RAS (several mm^2) and would therefore not contribute to the optical anisotropy.

Finding that the initial step of the deposition of aluminium on HOPG at -0.5 V is at least partially ordered, we are now investigating the influence of the different applied potentials on the deposition mechanism. To this end, a series of CA

measurements are performed. In this experimental series, the potential is first held at OCV for 60 s, then a cathodic potential is set for 60 s to observe the plating, followed by another OCV set for 60 s. For the stripping, the potential is set to 0.5 V (vs. Al pseudo-reference) for 90 s to ensure that all the plated Al is removed again from the surface. Finally, a last OCV step for 30 s is done. The cathodic potentials are -0.05 V, -0.075 V, -0.1 V, -0.15 V, -0.2 V, -0.3 V, -0.4 V, and -0.5 V, respectively. The measurements were all done in series, starting from the least to the most cathodic potential. During the CA measurements, anisotropy and reflectance transients were recorded at 1.5 eV. The results are displayed in Figure 4.

Figure 4d shows the DC-signal. Here, we observe three qualitatively different regimes, depending on the applied potential. At the less cathodic potentials (-0.05 V to -0.15 V), the reflectance decreases gradually after the potential is set to the desired voltage and the rate of decreasing reflectance increases with more cathodic potentials. It stays constant during the OCV phase and then increases again back to the initial value when applying the anodic voltage of 0.5 V. For the more cathodic potentials of -0.2 V and -0.3 V, there is an initial dip in the reflectance shortly after setting the potential. After the dip, it stays rather constant before there is again a dip when setting to +0.5 V. These dips are more pronounced for -0.3 V than for -0.2 V, but the reflectance recovers towards the end of the anodic potential step. For -0.4 V and -0.5 V, there is also a slight dip at the beginning, which is, however, less pronounced than for the previous two potentials. After this dip, the reflectance, however, increases and reaches values above the initial value at OCV. When setting the potential to 0.5 V, the reflectance decreases back to its original value, but also in a stepwise fashion with a small dip before reaching the plateau.

Under the assumption, that the reflectance decreases with increased (micro)roughness and vice versa, one can now derive

different plating and stripping regimes. For the low cathodic potentials and associated low current densities, surface roughness increases during plating and decreases during stripping, which is in line with Tu et al.^[38] This changes qualitatively for intermediate cathodic potentials (plating currents), where an initial phase of increasing roughness (especially for -0.3 V) is followed by a plating regime that then reduces surface roughness, for instance by plating a continuous film over coarse nucleation particles. The reverse is then observed for stripping, where roughness in an initial phase increases again. For the higher current densities then, the initial dip in reflectance again shows the nucleation phase, which is quickly followed a plating regime leading to a significantly enhanced reflectance, which one would expect for a flat, compact Al layer on top of the HOPG.

For the anisotropy (Figure 4c), there is almost no change for the less cathodic potentials of -0.05 V, -0.075 V, and -0.1 V, with only a shallow dip for the latter two potentials. Beyond -0.15 V, however, a pronounced negative anisotropy develops, which is very broad for -0.15 V and becomes more steep and narrow with increasing cathodic potential. After this initial peak, the anisotropy increases again and stays almost constant also during the OCV phase. During the stripping of the aluminium, there are narrow peaks between -0.15 and -0.3 V, a broad and late peak for -0.4 V and finally a very shallow and late peak for the sample plated with -0.5 V. This behaviour again suggests that for high plating current densities, a well-ordered nucleation phase exists, which is less ordered/pronounced at potentials less cathodic than -0.2 V. Though stripped at the same potential, these different plating regimes also translate to different behaviour in the stripping and, as for intermediate potentials, distinct negative peaks in the anisotropy can be observed. This suggests a qualitatively different microstructure

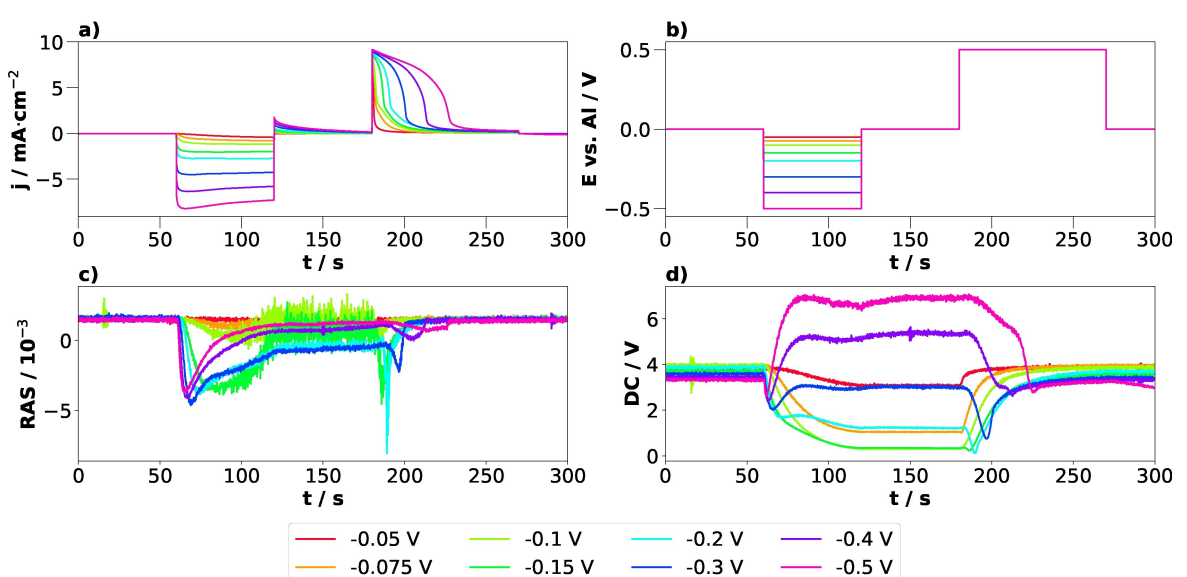


Figure 4. Aluminium deposition at different potentials (vs. Al pseudo-reference) as indicated by the colour code: a) current over time, b) voltage over time, c) RAS over time, d) DC over time. The results of one specific potential were recorded simultaneously. All potentials were recorded in series, starting from the least cathodic potential.

of the plated Al even in the plating regime at -0.4 V, where already a compact layer with increased reflectance is observed.

The different shapes of the reflectance and anisotropy spectra during aluminium plating and stripping strongly hint at qualitatively different plating and stripping mechanisms for different potentials. For an evaluation of the resulting macroscopic surface morphology, SEM/EDX measurements were performed at two distinct potentials, namely -0.1 V and -0.5 V (Figures 5 and 6). These two potentials were chosen because of their opposite features regarding anisotropy and reflectance. While for -0.1 V, there is a decrease in reflectance during plating and almost no anisotropy peak, -0.5 V shows an increase in reflectance while plating and a pronounced anisotropy peak at the beginning of Al deposition. For a better comparability, the same charge (250 mC) was deposited for both potentials.

Figure 5 shows the SEM/EDX image of the deposition of 250 mC at -0.1 V (23 min deposition time). The SEM image in part a) shows that tiny particles are distributed equally over the surface. In addition, there are also cauliflower-like bigger particles, which look like agglomerates of the smaller particles. The EDX mapping in Figure 5c confirms that the particles are indeed the deposited Al. The corresponding CC and transient diagram to this measurement can be found in the Supporting Information in Figure S6.

The SEM/EDX images of the Al deposition at -0.5 V (250 mC) (113 s deposition time) can be found in Figure 6. In

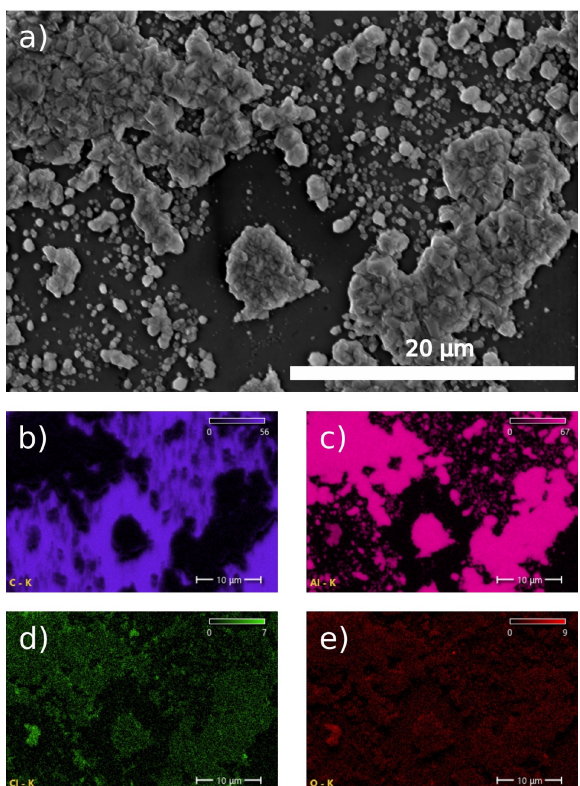


Figure 5. a) SEM images of the HOPG sample after deposition of Al 250 mC at -0.1 V (vs. Al pseudo-reference). EDX maps of b) carbon, c) aluminium, d) chloride, e) oxygen.

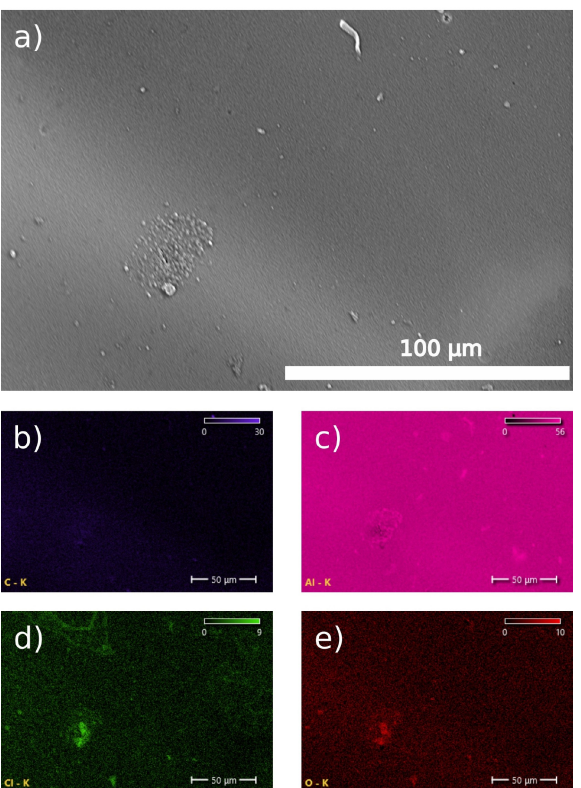


Figure 6. a) SEM images of the HOPG sample after deposition of Al 250 mC at -0.5 V (vs. Al pseudo-reference) EDX map of b) carbon, c) aluminium, d) chloride, e) oxygen.

contrast to the less cathodic potential, the SEM image in part a) now shows that the whole surface is more or less homogeneous, except for some tiny particles. The EDX analysis in parts b) to e) shows that the entire surface is covered with aluminium, which dampens the carbon signal. The corresponding CC and transient measurements are displayed in the Supporting Information in Figure S7.

Evaluating the results of anisotropy and reflectance during Al plating and the ex situ SEM/EDX images, we can now develop a more detailed hypothesis on the involved mechanism. A Volmer-Weber like growth (island growth) predominates at less cathodic potentials (-0.1 V), corroborated by the SEM image showing separate smaller and larger particles on the surface and the decreased reflectivity – increased roughness – during plating. For the more cathodic potentials (-0.5 V), however, Frank-van-der-Merwe like growth (layer-by-layer growth) after a short nucleation stage appears to dominate. This leads to the complete coverage of the HOPG surface with a dense, smooth and therefore optically lustrous Al layer. The optical anisotropy during plating suggests that the initial plating regime at high current densities involves a higher degree of ordering, i.e. well-defined nucleation as shown in Figure 3b, on the surface. This increases the roughness, which in turn leads to a decrease in reflectance. With further charge transferred, the particles – their shape suggests a close-packed (111) surface – start to merge, creating the dense Al layer.

Investigations by Tu et al.^[38] came to a similar conclusion for the electrodeposition of Al on graphite. The authors discovered that at low current density (16 mA cm^{-2}), the deposited Al becomes coarser, and the particles grow together and agglomerate. At the low current densities, the growth rate of nuclei is higher than the rate of new nuclei formation, leading to a coarse deposition.^[38,50] However, with increasing current density, there is a faster formation rate of new nuclei as compared with the growth rate of that, leading to fine-grained deposited particles.^[38,51] This leads to a uniform deposition and relatively smooth surface at high current density (32 and 57 mA cm^{-2}).^[38] From their findings, the authors proposed a potential mechanism for the Al deposition. This mechanism includes three steps. In the first step, a thin, compact Al layer is deposited on the electrode. In the second step, dendrites attach to the thin, compact layer. At high current density, fine-grained particles lead to high aluminium particle density. In contrast, at low current density, the coarse-grained particles result in a relatively high deformation. This makes it more likely for the foils to form dendrites. As a final step, the dendrites start to grow. Thereby, the growing particles fill up the interstices between the dendrites. This means that the fine-grained morphology at high current density is prone to form compact layers.^[38] This mechanism could explain why we see a compact Al layer at a higher cathodic potential (high current density) compared to a lower cathodic potential (low current density). However, we do not observe a film of Al on the surface at low potentials, at which the dendrites start to grow. One potential reason why we do not see a dense film of Al at less cathodic potential is that they used graphite while we used HOPG. This means that they start from surface with higher roughness and, therefore, more potential nucleation spots compared to our HOPG. Another reason could be the different electrolytes: While their study employed [Bmim]Cl, we used [EMImCl]AlCl₃. The high roughness, Munoz-Tornero et al.^[13] discovered during their electrodeposition of Al on expanded graphite, could be explained by the fact that they used expanded graphite compared to HOPG. In addition, their deposition time was 180 min (at -0.5 mA cm^{-2}), much longer than our experiments, which might lead to different morphologies.

Conclusions

We have used *operando* reflection anisotropy spectroscopy to investigate the stripping and plating of aluminium from the ionic liquid [EMImCl]:AlCl₃ onto highly-oriented pyrolytic graphite in a time-resolved manner. The approach also allowed us to observe the formation of a stable SEI on HOPG in parallel to the intercalation of AlCl₄⁻ into the graphite structure. We showed that at less cathodic potentials, there is the formation of Al-islands on the surface, which are, for intermediate potentials, plated over with an Al layer of intermediate roughness. For more cathodic potentials, on the other hand, a compact and smooth Al-layer is formed on the surface after an initial nucleation phase with a high degree of ordering. These different plating regimes also lead to distinct stripping, where

the Al layer deposited at -0.5 V appears to feature the most homogeneous stripping behaviour. For the function of the graphite as cathode, we observed that during the first cycle going above 1.8 V , both an irreversible swelling of the topmost layer of the graphic, as well as formation of a stable surface layer, occurs. For subsequent cycles at potentials above 1.8 V , the reversible ad-, desorption or intercalation of AlCl₄⁻ is associated with distinct optical signatures.

This work shows the potential of electrochemical RAS as an *operando* technique for the investigation of battery interfaces, probing in a time-resolved manner to what extent (fast) charging routines lead to or avoid dendrite formation and, as a consequence of this, cause cell damage. Once a reliable understanding of spectra-structure relationships is formed, models can be developed^[52] that enable real-time *operando* control of surface morphologies as a function of electrochemical parameters. With time-resolutions of commercial spectrometers in the range of 10 ms, the approach could also provide valuable insight for the investigation of metal deposition via pulsed current, avoiding dendrite formation.^[53]

Further research should also be dedicated to AlCl₃-free electrolytes in Al dual-graphite batteries, since AlCl₃-based electrolytes are known to be corrosive towards cell parts.^[6] While AlCl₃-free electrolytes have the disadvantage that plating and stripping onto metal aluminium is challenging,^[8,54] the use of graphite as an anode would circumvent this issue and render AlCl₃-free electrolytes more promising candidates for Al-based batteries.

Experimental Section

Materials and Electrolyte Preparation

A plate of highly-oriented pyrolytic graphite (HOPG) with the dimensions of $10 \text{ mm} \times 10 \text{ mm} \times 1 \text{ mm}$ and a mosaic angle of $0.8 \pm 0.2^\circ$ was purchased from Thermo Scientific. For a reproducible surface for each experiment, the topmost layer was removed with adhesive tape from Tesa. For the electrolyte preparation, [EMImCl]:AlCl₃ (1:1.5) was prepared by slowly adding aluminium chloride (AlCl₃) (Anhydrous, Sigma-Aldrich, 99.99%) to 1-Ethyl-3-methylimidazolium chloride (EMImCl) (Sigma-Aldrich, >95%) while stirring with a magnetic stirring bar at room temperature (28 to 30°C) inside an argon-filled glovebox (MBraun, <1 ppm O₂, <1 ppm H₂O). Anhydrous Tetrahydrofuran (THF) (99.8%) was purchased from Sigma-Aldrich.

Electrochemical Setup

All electrochemical experiments were performed inside an argon-filled glovebox. The electrochemical measurement was conducted using a photo-electrochemical cell (PEC cell) from Zahner. An Al wire from Alfa Aesar (0.5 mm diameter, 99.9999% purity) was used as a pseudo-reference electrode. The cell was filled with 1.5 ml of [EMImCl]:AlCl₃ (1:1.5) to ensure HOPG and Al-wire were covered with electrolyte, but the electrolyte layer was thin enough not to cause too much light absorption. The electrochemical measurements were controlled with a Gamry Instruments potentiostat (Interface 5000E). For the deposition experiments, three activating cycles were performed first, between 0.5 V and 1.5 V, starting from OCV towards the negative terminus with a scan rate of 10 mV^{-1} .

Reflection Anisotropy Measurements

For the RA measurement, an EpiRAS from Laytec was employed. For measurements inside the glovebox, the spectrometer was installed on top of the glovebox with a quartz window placed in the sealing of the glovebox between the setup and the spectrometer, allowing light transmission. The electrochemical cell was placed under the window on top of a hexapod (Physik Instrumente H-840), which allowed for rotating, inclining, and translating the cell to align it with the lightpath. For the SEM/EDX measurements, the Apero 2 from Thermo Fisher Scientific with the clean connect system was utilized. This system facilitated the transfer of the sample from the glovebox to the SEM without compromising the inert environment. For a reproducible orientation of the sample, one edge was marked, allowing for the same orientation of the sample in every experiment. The HOPG had a low reflectivity, in order to measure RAS spectra, the reflected lightpath did not go via the anti-wobble-mirror but directly into the detector. To still obtain correct RAS values, the measured RAS was multiplied by a factor of 2. A baseline correction was applied to all the spectra using an optically isotropic Si(100) sample inside the glovebox. The SEM/EDX measurements were carried out using a 10 kV electron beam and a beam current of 26 nA.

Acknowledgements

This research was funded by the Deutsche Forschungsgemeinschaft (DFG, German Research Foundation) under Germany's Excellence Strategy – EXC 2154 – Project number 390874152 and DFG project 434023472. Open Access funding enabled and organized by Projekt DEAL.

Conflict of Interests

The authors declare no conflict of interest.

Data Availability Statement

The data that support the findings of this study are available at Zenodo at <https://doi.org/10.5281/zenodo.13270220>.^[55]

Keywords: aluminium batteries · electrodeposition · HOPG · solid electrolyte interface · reflection anisotropy spectroscopy

- [1] S. K. Gupta, J. Vishwakarma, A. K. Srivastava, C. Dhand, N. Dwivedi, *Energy Storage Mater.* **2024**, *70*, 103538.
- [2] X. Zhang, R. Lv, W. Tang, G. Li, A. Wang, A. Dong, X. Liu, J. Luo, *Adv. Funct. Mater.* **2020**, *30*.
- [3] J. Tu, W.-L. Song, H. Lei, Z. Yu, L.-L. Chen, M. Wang, S. Jiao, *Chem. Rev.* **2021**, *121*, 4903.
- [4] S. K. Das, S. Mahapatra, H. Lahan, *J. Mater. Chem. A* **2017**, *5*, 6347.
- [5] H. Chen, H. Xu, B. Zheng, S. Wang, T. Huang, F. Guo, W. Gao, C. Gao, *ACS Appl. Mater. Interfaces* **2017**, *9*, 22628.
- [6] E.-S. Lee, S.-H. Huh, S.-H. Lee, S.-H. Yu, *ACS Sustain. Chem. Eng.* **2023**, *11*, 2014.
- [7] G. Studer, A. Schmidt, J. Büttner, M. Schmidt, A. Fischer, I. Krossing, B. Esser, *Energy Environ. Sci.* **2023**, *16*, 3760.
- [8] F. Rahide, J. K. Flowers, J. Hao, H. S. Stein, H. Ehrenberg, S. Dsoke, *J. Electrochem. Soc.* **2023**, *170*, 120534.
- [9] M. Kliment, M. V. Kovalenko, K. V. Kravchyk, *Commun. Chem.* **2022**, *5*.
- [10] X. Huang, Y. Liu, C. Liu, J. Zhang, O. Noonan, C. Yu, *CChem. Sci.* **2018**, *9*, 5178.
- [11] R. Buckingham, T. Asset, P. Atanassov, *J. Power Sources* **2021**, *498*, 229762.
- [12] R. Tao, H. Fu, C. Gao, L. Fan, E. Xie, W. Lyu, J. Zhou, B. Lu, *Adv. Funct. Mater.* **2023**, *33*.
- [13] D. Muñoz-Torero, P. Leung, E. García-Quismondo, E. Ventosa, M. Anderson, J. Palma, R. Marcilla, *J. Power Sources* **2018**, *374*, 77.
- [14] Z. Li, J. Liu, B. Niu, J. Li, F. Kang, *Small* **2018**, *14*.
- [15] S. Wang, S. Jiao, W.-L. Song, H.-S. Chen, J. Tu, D. Tian, H. Jiao, C. Fu, D.-N. Fang, *Energy Storage Mater.* **2018**, *12*, 119.
- [16] M. Tebyetekerwa, T. T. Duignan, Z. Xu, X. Song Zhao, *Adv. Energy Mater.* **2022**, *12*.
- [17] S. Chen, Q. Kuang, H. J. Fan, *Small* **2020**, *16*.
- [18] Q. Zhou, Y. Zheng, D. Wang, Y. Lian, C. Ban, J. Zhao, H. Zhang, *Ceram. Int.* **2020**, *46*, 26454.
- [19] P. Bhauriyal, A. Mahata, B. Pathak, *Phys. Chem. Chem. Phys.* **2017**, *19*, 7980.
- [20] M.-C. Lin, M. Gong, B. Lu, Y. Wu, D.-Y. Wang, M. Guan, M. Angell, C. Chen, J. Yang, B.-J. Hwang, H. Dai, *Nature* **2015**, *520*, 324.
- [21] N. Canever, F. R. Hughson, T. Nann, *ACS Appl. Energy Mater.* **2020**, *3*, 3673.
- [22] W. A. Appiah, A. Stark, S. Lysgaard, J. Busk, P. Jankowski, J. H. Chang, A. Bhowmik, B. Gollas, J. M. Garcia-Lastra, *Chem. Eng. J.* **2023**, *472*, 144995.
- [23] V. Elterman, P. Shevelin, L. Yolshina, A. Borozdin, *Electrochim. Acta* **2021**, *389*, 138715.
- [24] R. Böttcher, S. Mai, A. Ispas, A. Bund, *J. Electrochem. Soc.* **2020**, *167*, 102516.
- [25] K. Uji, S. Kobayashi, K. Sasaki, T. Takeguchi, T. Tsuda, M. Ueda, J. Nunomura, Y. Honkawa, Y. Kojima, *J. Electrochem. Soc.* **2021**, *168*, 056510.
- [26] T. Jiang, M. Chollier Brym, G. Dubé, A. Lasia, G. Brisard, *Surf. Coat. Technol.* **2006**, *201*, 1.
- [27] T. Schoetz, O. Leung, C. P. de Leon, C. Zaleski, I. Efimov, *JES* **2020**, *167*, 040516.
- [28] T. Brülle, U. Stimming, *J. Electroanal. Chem.* **2009**, *636*, 10.
- [29] A. N. Simonov, O. V. Cherstouk, S. Y. Vassiliev, V. I. Zaikovskii, A. Y. Filatov, N. A. Rudina, E. R. Savinova, G. A. Tsirlina, *Electrochim. Acta* **2014**, *150*, 297.
- [30] C. Zhong, W. Hu, Y. Cheng, *J. Power Sources* **2011**, *196*, 8064.
- [31] R. Pötzschke, C. Gervasi, S. Vinzelberg, G. Staikov, W. Lorenz, *Electrochim. Acta* **1995**, *40*, 1469.
- [32] D. Salinas, E. Cobo, S. Garcia, J. Bessone, *J. Electroanal. Chem.* **1999**, *470*, 120.
- [33] M. Kettner, C. Stumm, M. Schwarz, C. Schuschke, J. Libuda, *Surf. Sci.* **2019**, *679*, 64.
- [34] J. H. Um, S. Yu, *Adv. Energy Mater.* **2020**, *11*.
- [35] L. Leuppert, A. Reupert, T. Diemant, T. Philipp, C. Kranz, Z. Li, M. Fichtner, *RSC Applied Interfaces* **2024**.
- [36] D.-M. She, W.-L. Song, J. He, N. Li, H. Chen, S. Jiao, D. Fang, *JES* **2020**, *167*, 130530.
- [37] M. S. Ding, T. Diemant, R. J. Behm, S. Passerini, G. A. Giffin, *JES* **2018**, *165*, A1983.
- [38] X. Tu, J. Zhang, M. Zhang, Y. Cai, H. Lang, G. Tian, Y. Wang, *RSC Adv.* **2017**, *7*, 14790.
- [39] B. Scharifker, G. Hills, *Electrochim. Acta* **1983**, *28*, 879.
- [40] M. M. May, W. Jaegermann, *Curr. Opin. Electrochem.* **2022**, *34*, 100968.
- [41] M. Guidat, M. Löw, M. Kölbach, J. Kim, M. M. May, *ChemElectroChem* **2023**, *10*, e202300027.
- [42] K. Haberland, P. Kurpas, M. Pristovsek, J.-T. Zettler, M. Weyers, W. Richter, *Appl. Phys. A* **1999**, *68*, 309.
- [43] M. Guidat, F. Rahide, M. Löw, J. Kim, H. Ehrenberg, S. Dsoke, M. M. May, *Batter. Supercaps* **2024**, *7*, e202300394.
- [44] E. A. Schmitt, M. Guidat, M. Nußhör, A.-L. Renz, K. Möller, M. Flieg, D. Lörch, M. Kölbach, M. M. May, *Cell Rep. Phys. Sci.* **2023**, *4*, 101606.
- [45] A. Kotronia, H. D. Asfaw, C.-W. Tai, M. Hahlin, D. Brandell, K. Edström, *ACS Appl. Mater. Interfaces* **2021**, *13*, 3867.
- [46] E. Peled, S. Menkin, *J. Electrochem. Soc.* **2017**, *164*, A1703.
- [47] J. Zhao, C. Zhao, C. Zou, Y. Wang, W. Wang, Q. Peng, Y. Li, S. Han, L. Zhang, *ChemSusChem* **2023**, *17*.
- [48] R. S. Berry, B. M. Smirnov, *J. Chem. Phys.* **2000**, *113*, 728.
- [49] A. Ishii, *Comput. Mater. Sci.* **2025**, *246*, 113342.
- [50] V. Kamavaram, D. Mantha, R. Reddy, *J. Min. Metall. Sect. B* **2003**, *39*, 43.
- [51] Y. Chao-Cheng, *Mater. Chem. Phys.* **1994**, *37*, 355.

- [52] E. Oliveira, J. Strassner, C. Doering, H. Fouckhardt, *Appl. Surf. Sci.* **2023**, 611, 155769.
- [53] K. Cicvarić, S. Pohlmann, B. Zhang, F. Rahamanian, L. Merker, M. Gaberšček, H. S. Stein, *Phys. Chem. Chem. Phys.* **2024**, 26, 14713.
- [54] M. Talarí, A. Sarapulova, E. Zemlyanushin, N. Sabi, A. Hofmann, V. Trouillet, S. Dsoke, *Batter. Supercaps* **2024**.
- [55] M. Löw, M. M. May, Dataset for "Operando investigation of Al plating regimes on HOPG in [EMImCl]:AlCl₃ by electrochemical reflection anisotropy spectroscopy" 2024, <https://doi.org/10.5281/zenodo.13270220>.

Manuscript received: September 16, 2024
Revised manuscript received: October 21, 2024
Accepted manuscript online: October 22, 2024
Version of record online: November 14, 2024
